

15. A. M. Perelomov, V. S. Popov, and M. V. Terent'ev, *Sov. Phys. JETP* **23**, 924 (1966).
16. R. L. Kelly and L. J. Palumbo, *Atomic and Ionic Emission Lines Below 2000 Angstroms: Hydrogen Through Krypton* (U.S. Govt. Print. Off., Naval Research Laboratory, Washington, DC, 1973).

## 1.E Femtosecond Nonlinearities and Hot-Carrier Dynamics in GaAs

The properties of hot carriers are determined primarily by the electronic band structure of the host material and carrier-lattice and carrier-carrier interactions—topics that have historically been of sustained interest in solid-state physics. Because of the continuing size reduction of conventional semiconductor devices and the emergence of new devices based upon advanced growth techniques, the study of hot-carrier dynamics remains of importance. Current research on hot-carrier dynamics relies on optical techniques, often using light both as an injector of relatively mono-energetic electrons and as a probe of the carrier distribution. The advent of ultrashort laser pulses provides a very direct means of investigating hot-carrier relaxation and cooling processes with excellent temporal resolution.

Extensive investigations of hot-carrier dynamics in GaAs have been performed using ultrafast spectroscopy.<sup>1-14</sup> In this article, we present a new series of studies of hot-carrier dynamics. The transient absorptive and refractive nonlinearities of GaAs have been measured with a temporal resolution of less than 100 fs. Various hot-carrier processes and their influences on the ultrafast optical response are discussed.

### Techniques

We have used a copper-vapor, laser-amplified CPM laser to perform pump-probe measurements on GaAs at room temperature. About 3% of the 75- to 100-fs pulses at 620 nm is used as the pump beam. The remainder is focused onto a jet of ethylene glycol, producing a white-light continuum, which is used as a probe pulse. The probe wavelength is selected with interference filters over a spectral region from 550 nm to 950 nm. The polarization of the pump and probe pulses is orthogonal to reduce coherent artifacts. The intensity of the pump pulse can be varied over nearly two orders of magnitude.

The time-resolved transmission  $T(t)$  and reflection  $R(t)$  are measured simultaneously on a thin ( $<0.3\text{-}\mu\text{m}$ ) intrinsic GaAs film obtained using a lift-off technique<sup>15</sup> and attached to a sapphire window. The absorption coefficient  $\alpha(t)$  and refractive index  $n(t)$  are then deduced from the measured  $T$  and  $R$  by inversion of the Fabry-Perot formulae. The changes of refractive index  $\Delta n(t)$  are also obtained by measuring the time-resolved differential reflection  $\Delta R/R$  on thick GaAs samples.<sup>13</sup>

## Results

### 1. Refractive-Index, Spectral-Hole Burning

For excitation of GaAs at 2 eV (620 nm), the electrons are initially injected into the  $\Gamma$  valley at the three distinct excess energies of 0.50 eV, 0.43 eV, and 0.15 eV, caused by transitions from the heavy-hole, light-hole, and split-off valence bands with a relative strength of 42%, 42%, and 16%, respectively. The transient decrease of absorption, caused by the nonthermal carrier distribution generated after femtosecond excitation, is characterized by an absorption spectral hole near 2 eV.<sup>6,16</sup> According to the Kramers-Kronig relation, the existence of a spectral hole in the imaginary part of the refractive index (absorption) will cause a spectral resonance in the change of a real part of the refractive index. We have indeed observed this resonance around 2 eV, which we call refractive-index, spectral-hole burning.<sup>13</sup> Figure 50.24 shows our measurements of the spectral dependence of the refractive-index change for  $N \sim 2.5 \times 10^{18} \text{ cm}^{-3}$ . As shown in Fig. 50.24(b), the spectral hole disappears quickly because a large fraction of the electrons scatter to the  $X$  and  $L$  valleys and the rest thermalize within the  $\Gamma$  valley on a sub-100-fs time scale.

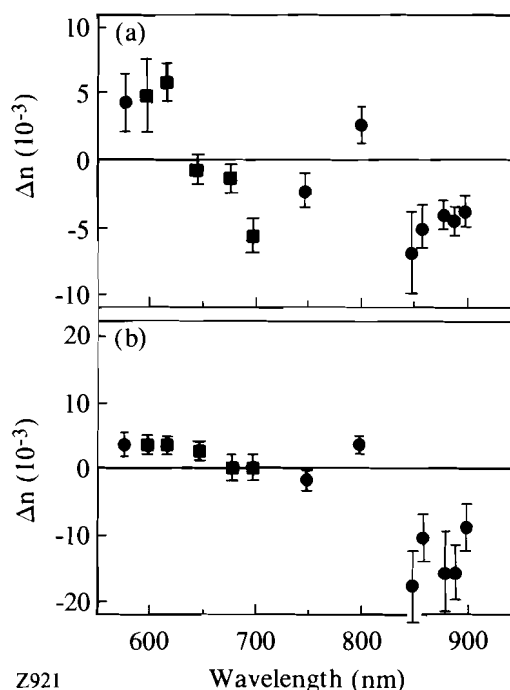


Fig. 50.24

Measured  $\Delta n$  spectrum for  $N \sim 2.5 \pm 1.2 \times 10^{18} \text{ cm}^{-3}$  at time delays: (a)  $t \sim 0^+$  and (b)  $t \sim 200^+$  fs. Squares are the measured average values for both a film and a bulk sample; circles are the measured average values for a thin film. The error bars are obtained from the standard deviation of the measured values and a conservative estimate of the uncertainty in carrier density. A clear spectral resonance around 620 nm appears in (a).

If the absorption spectral hole burned at  $t \sim 0^+$  followed the symmetric pump spectrum around 620 nm (2 eV), we expect that the change of the refractive index would be zero at 620 nm. However, our data clearly show that the zero change of the refractive index is near 650 nm, and not at 620 nm. Furthermore, measurements on the absorption changes also confirm that at  $t \sim 0^+$ ,  $|\Delta\alpha|$  is larger near 650 nm than at 620 nm, a result that can also be inferred from absorption

spectral-hole-burning measurements made around 620 nm by others.<sup>16</sup> Therefore, on a time scale shorter than our temporal resolution, the initial excited carrier “distribution” is strongly deformed and becomes spectrally asymmetric, and the peak of the distribution appears to be red-shifted. The  $\Gamma$ -valley electrons excited from the heavy-hole valence band by 2-eV photons can scatter to both  $X$  and  $L$  valleys; by contrast, those electrons excited from the light-hole valence band can only scatter to the  $L$  valley. Therefore, the electrons excited from the heavy-hole valence band are more likely to be transferred to the satellite valleys than those excited from the light-hole valence band. This “preferred” scattering produces a deformation of the excited-carrier distribution. This process also appears to be instantaneous within our temporal resolution because carriers excited by the earlier part of the pump pulse have already started undergoing this effect. Another effect, which was recently observed and termed “resonant intervalley scattering” by Bigot *et al.*,<sup>17</sup> can also contribute to the ultrafast deformation (shift) of the absorption spectral hole. Because of the vanishing density of  $|X\rangle$  states at the  $\Gamma$ - $X$  transition point, the return of electrons from the bottom of the  $X$  valley to the  $\Gamma$  valley is more probable, thereby enhancing the concentration of electrons in the  $\Gamma$  valley near the transition point. We note that the peak of the “trapped” electron distribution ( $\sim 1.92$  eV or 646 nm, 30 meV below the  $X$ -valley minimum) is very close to the zero change of the refractive-index spectral resonance. It is still not clear why this resonant process takes place in  $\sim 50$  fs<sup>17</sup> because an electron has to emit or absorb a phonon twice in order to complete this process. Nevertheless, this explanation is supported by the following facts: the shift has little carrier-density dependence; it does not appear<sup>3</sup> or is very small<sup>18</sup> when the spectral hole is burned below the  $L$ -valley minimum; it does not appear in InP,<sup>19</sup> a material in which there is no intervalley scattering with 620-nm excitation; and  $\Delta n$  is nearly zero at the pump wavelength (620 nm) at  $t \sim 0+$  for GaAs at low temperature (2 K)<sup>20</sup> when the  $\Gamma$ - $X$  transition is suppressed.

## 2. Studies of the Initial Scattering Time

If pump-probe measurements are performed at the same wavelength, the recovery of the bleaching measures the scattering rate of carriers from the initially optically coupled states. Since  $\Delta n(t)$  measures the spectrally integrated population change near the as-excited states, it is best to use  $\Delta\alpha(t)$  to deduce the initial scattering time. Figure 50.25 shows  $\Delta\alpha(t)$  at 620 nm for various injected-carrier densities.

We have developed a simplified model in which the initial fast bleaching is modeled by two equations

$$\frac{dN}{dt} = \frac{N_0 I_{\text{pump}}(t)}{\int_{-\infty}^{+\infty} I_{\text{pump}}(t) dt} - \frac{N}{\tau_T} \quad (1)$$

$$S(t) \propto \int_{-\infty}^{+\infty} I_{\text{probe}}(t'-t) N(t') dt, \quad (2)$$

where  $N_0$  is the total injected-carrier density,  $N$  is the time-dependent carrier density in the excited states,  $1/\tau_T$  is an effective total scattering rate from the initial excited states,  $I_{\text{pump}}(t) = I_{\text{probe}}(t) = \text{sech}^2(1.763 t/\tau_p)$ , and  $S(t)$  is the detected signal. If  $\tau_T \gg \tau_p$ , the decay part of  $N(t)$  can be simply described by an exponential with time constant  $\tau_T$ . However, when  $\tau_T \sim \tau_p$ , as in our measurements,  $N(t)$  does not have a simple form.

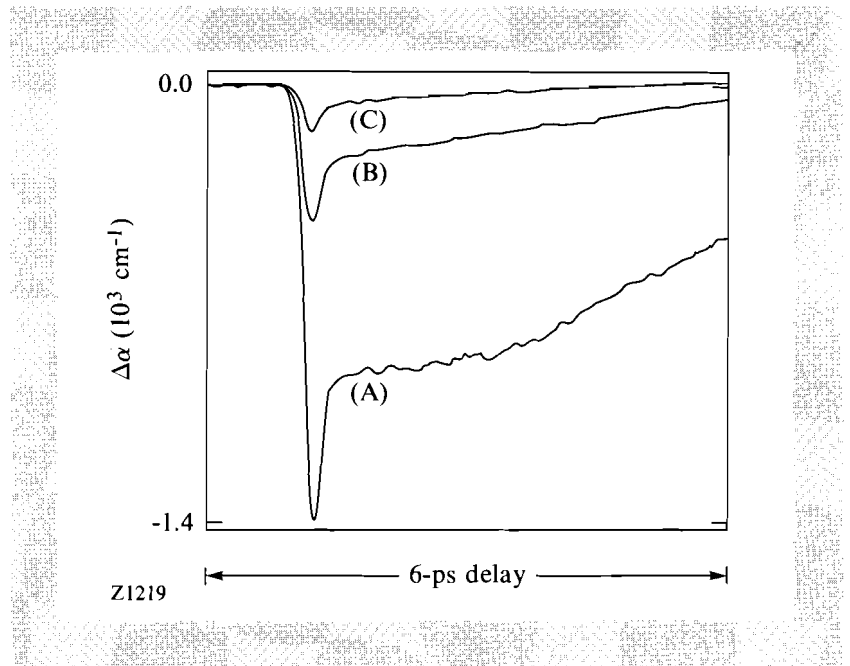


Fig. 50.25  
Time evolution of  $\Delta\alpha$  at 620 nm for different  $N \sim$ : (A)  $3.3 \times 10^{18} \text{ cm}^{-3}$ , (B)  $9.5 \times 10^{17} \text{ cm}^{-3}$ , and (C)  $3 \times 10^{17} \text{ cm}^{-3}$ .

From Fig. 50.25, it is clear that the change of the signal is not governed by a single decay process, but rather that a fast process is superimposed on a much slower variation. It is important to note that the slow variation is rather different at each carrier density. This result prevents the traces obtained for different carrier densities from being normalized by the amplitudes of their slow variations, a method used by others.<sup>6</sup> However, at least for low carrier densities ( $N < 5 \times 10^{17} \text{ cm}^{-3}$ ), the slow variation of  $\Delta\alpha(t)$  is well described by an exponential decay. The solid line shown in Fig. 50.26(a) is a fit of the slow decay of  $\Delta\alpha(t)$  for  $N \sim 3 \times 10^{17} \text{ cm}^{-3}$  using Eqs. (1) and (2) with  $\tau_p = 100 \text{ fs}$  and  $\tau_{T2} = 2 \text{ ps}$ . This slow component is subtracted from the experimental trace to obtain the “effective” fast bleaching component, as shown by a dotted line in Fig. 50.26(b). We then use Eqs. (1) and (2) again to fit the fast bleaching. The solid line shown in Fig. 50.26(b) is the best fit using  $\tau_p = 100 \text{ fs}$  and  $\tau_{T1} = 50 \text{ fs}$ .

It is worth mentioning that only less than 35% of the total excited electrons ever accumulate in the “as-excited” states; most of them have already scattered away within the pulse width since  $\tau_{T1} \sim 0.5 \tau_p$ . After  $\sim 200 \text{ fs}$ , the split-off probe makes a major contribution to  $\Delta\alpha$ ; it monitors the band filling and the cooling of the  $\Gamma$ -valley electron distribution  $\sim 150 \text{ meV}$  above the conduction-band edge. The fact that the split-off probe samples the Boltzmann “tail” for low carrier densities ( $< 5 \times 10^{17} \text{ cm}^{-3}$ ) is probably responsible for the exponential decay of the slow component.

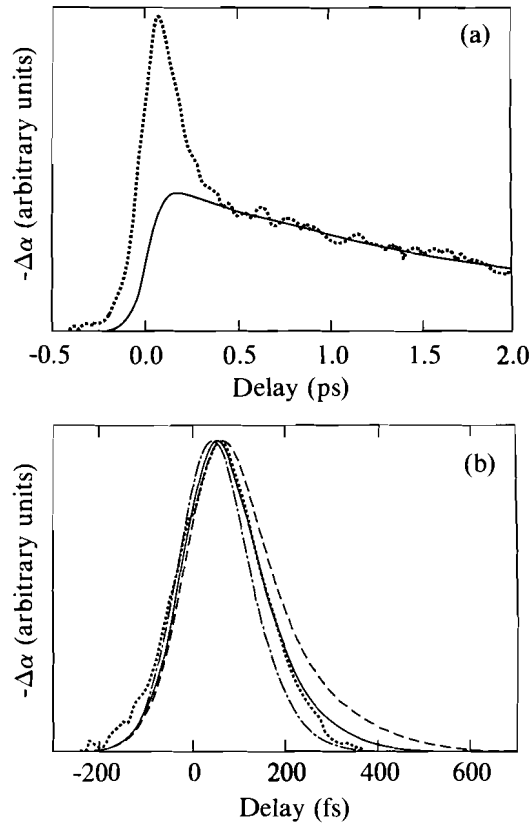


Fig. 50.26

(a) Measured time-resolved  $\Delta\alpha$  at 620 nm for  $N \sim 3 \times 10^{17} \text{ cm}^{-3}$  (dotted line) and a fit (solid line) for a slow decay with  $\tau_p = 100$  fs and  $\tau_{T2} = 2$  ps; (b) The fast component (dotted line), obtained by subtracting a slow component [solid line in (a)] from the experimental curve [dotted line in (a)], is compared to different fits with  $\tau_p = 100$  fs and  $\tau_{T1} = 50$  fs (solid line),  $\tau_T = 70$  fs (dashed line), and  $\tau_T = 30$  fs (dashed-dotted line). The best fit is obtained using  $\tau_{T1} = 50$  fs.

Z1221

At higher carrier densities, the slow component is rather complicated and the simple fit described previously does not work well. However, information on the initial effective scattering rate can be obtained by monitoring the peak value of the transient spike of  $\Delta\alpha(t)$  as a function of carrier density. Figure 50.27 plots  $|\Delta\alpha_{\text{max}}|$  versus  $N$ . The weak sublinearity of the data indicates that  $\tau_T$  decreases little at higher carrier densities:  $\tau_T$  is reduced from  $\sim 50$  fs to  $\sim 40$  fs when  $N$  increases from  $3 \times 10^{17} \text{ cm}^{-3}$  to  $7 \times 10^{18} \text{ cm}^{-3}$ . The value of  $\tau_T$  at high  $N$  ( $\sim 40$  fs) is very close to the values obtained by other groups with a three-time-component fit<sup>2,9</sup> or a similar two-time-component fit.<sup>21</sup>

We now consider the microscopic origin of the ultrafast initial scattering time. The contributions by electrons excited from the heavy-hole, light-hole, and split-off valence bands all need to be considered. Intervalley scattering is a very important process, and its rate is currently under investigation.<sup>22</sup> Recently Zollner *et al.*<sup>23</sup> introduced the concept of an effective intervalley deformation potential (IDP) in which the contribution of the TA phonons is included in a temperature-dependent IDP for LO-phonon scattering. If we use values of Zollner *et al.* ( $D_{\Gamma L} \sim 5.8 \times 10^8 \text{ eV/cm}$  and  $D_{\Gamma X} \sim 9.4 \times 10^8 \text{ eV/cm}$  at  $T_L = 300 \text{ K}$ ) to calculate the intervalley scattering times at different excited energies, we obtain  $\tau_{\Gamma X}(\sim 0.5 \text{ eV}) \sim 130$  fs,  $\tau_{\Gamma L}(\sim 0.5 \text{ eV}) \sim 120$  fs, and  $\tau_{\Gamma L}(\sim 0.43 \text{ eV}) \sim 150$  fs.

$\tau_{LO}$  (the unscreened LO-phonon emission time) is taken to be  $\sim 180$  fs.<sup>4,24</sup> The effective initial scattering time is then given by

$$\frac{1}{\tau_T} = 0.42 \left( \frac{1}{\tau_{\Gamma X}(0.5 \text{ eV})} + \frac{1}{\tau_{\Gamma L}(0.5 \text{ eV})} + \frac{1}{\tau_{LO}} \right) + 0.42 \left( \frac{1}{\tau_{\Gamma L}(0.43 \text{ eV})} + \frac{1}{\tau_{LO}} \right) + 0.16 \left( \frac{1}{\tau_{LO}} \right). \quad (3)$$

The calculated value of 65 fs is close to the measured  $\tau_T \sim 50$  fs at  $N \sim 3 \times 10^{17} \text{ cm}^{-3}$ . The 30% difference can be attributed to carrier-carrier scattering. The fact that  $\tau_T$  only decreases to  $\sim 40$  fs at high  $N$  points out that carrier-carrier scattering does not strongly affect the initial scattering time, a conclusion also reached by others.<sup>2,9</sup>

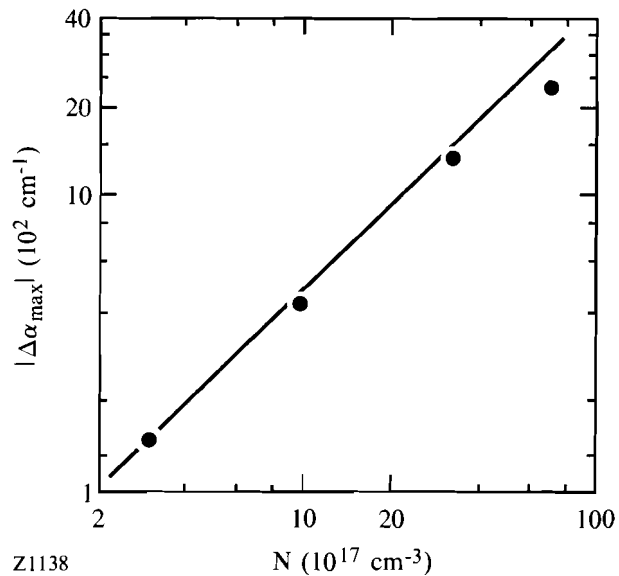


Fig. 50.27  $|\Delta\alpha_{\max}|$  ( $t \sim 0^+$ ) as a function of  $N$  at 620 nm. The straight line represents a linear relationship between  $|\Delta\alpha_{\max}|$  and  $N$ .

### 3. Band-Edge Nonlinearities

The interactions between hot carriers strongly affect absorptive and refractive nonlinearities around the band edge. Figure 50.28 shows the time-resolved changes of absorption for the same carrier density ( $N \sim 1.5 \pm 0.7 \times 10^{18} \text{ cm}^{-3}$ ) at probe wavelengths of 880, 890, 900, and 920 nm, which are below the band edge, and of 860 nm, which is slightly above the band edge. The short-lived increase of absorption observed at 880, 890, and 900 nm right after excitation is attributed

to band-gap renormalization accompanied by plasma screening of Coulomb interactions. Coulomb screening is often neglected in the interpretation of many experiments. The decrease of absorption slightly above the band edge (850 and 860 nm) immediately after excitation, which is caused by the reduction of Coulomb (Sommerfeld) enhancement factor, reveals the importance of this effect. Plasma screening of Coulomb interactions, along with band-gap renormalization, causes a clear spectral resonance in  $\Delta\alpha$  around the band edge, which takes place instantaneously when most carriers are still “hot”.<sup>11</sup> The subsequent broadband decrease of absorption indicates that the states near the perturbed band edge become filled.

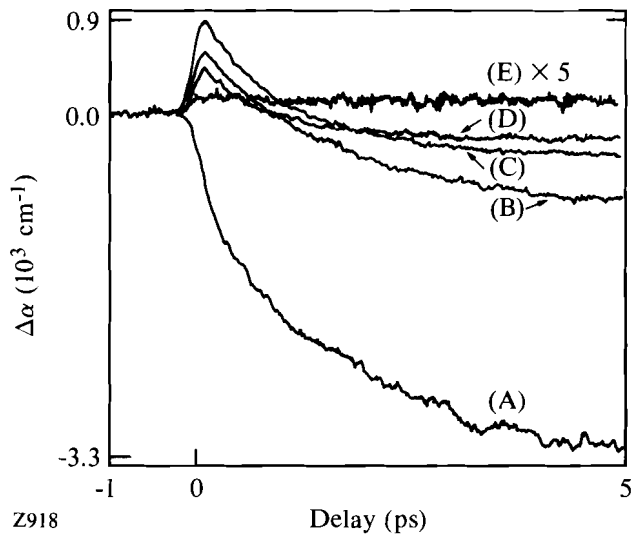


Fig. 50.28

Measured, time-resolved  $\Delta\alpha$  for  $N \sim 1.5 \pm 0.7 \times 10^{18} \text{ cm}^{-3}$ . The probe wavelengths are: (A) 860 nm, (B) 880 nm, (C) 890 nm, (D) 900 nm, and (E) 920 nm. Curve (E) has been multiplied by 5.

At 920 nm ( $\sim 75$  meV below the original band edge), a small, long-lived induced absorption is observed. This effect is attributed to intra-band (free-carrier) absorption. We investigate it by probing at 950 nm, which is  $\sim 120$  meV below the original band edge. Figure 50.29(a) and 50.29(b) show  $\Delta\alpha(t)$  and  $\Delta n(t)$  for various (high) carrier densities. Both  $|\Delta\alpha_{\text{max}}|$  and  $|\Delta n_{\text{max}}|$  scale approximately linearly with  $N$ , consistent with free-carrier absorption (FCA) being the main contribution to the nonlinearities at this wavelength. The cross section for FCA, defined as  $\sigma_{eh} = \Delta\alpha/N$ , is  $\sim 2.6 \pm 1.0 \times 10^{-17} \text{ cm}^2$  at 950 nm. Free-carrier absorption in  $n$ -type GaAs has been systematically studied earlier,<sup>25</sup> and  $\sigma_e$  (solely because of electrons) deduced from those data is  $\sim 8 \times 10^{-18} \text{ cm}^2$ . Other measurements<sup>25,26</sup> also show that  $\sigma_h$  (solely caused by holes) is more than a factor of 2 larger than  $\sigma_e$ . Our estimated  $\sigma_{eh}$  is close to  $\sigma_e + \sigma_h$ . It is interesting to note that  $\sim 5$  ps after excitation, when the carriers are cooled down,  $\Delta\alpha$  is only  $\sim 20\%$  smaller than after  $< 0.5$  ps, when the carriers are still hot<sup>27</sup> and many of them reside in the satellite valleys. Also, 950 nm  $|\Delta n|$  is quite large because band filling causes a large negative  $\Delta n$ , which extends far below the band edge.<sup>28</sup> Such large refractive nonlinearities should be useful for designing optoelectronic devices such as phase modulators.

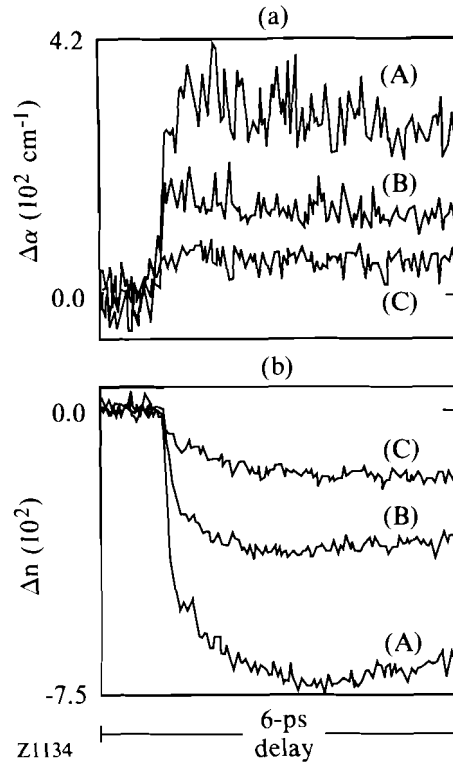


Fig. 50.29

Measured, time-resolved (a)  $\Delta\alpha$  and (b)  $\Delta n$  at 950 nm for various  $N$ : (A)  $1.3 \times 10^{19} \text{ cm}^{-3}$ , (B)  $5 \times 10^{18} \text{ cm}^{-3}$ , (C)  $2 \times 10^{18} \text{ cm}^{-3}$ .

#### 4. Band-Edge Gain Dynamics

For high injected-carrier densities ( $N > 10^{18} \text{ cm}^{-3}$ ), the combination of nearly instantaneous intra- $\Gamma$ -valley redistribution of electrons<sup>12,23</sup> with the rapid scattering of the high-energy  $\Gamma$ -valley electrons to the  $X$  and  $L$  valleys<sup>10</sup> should make it possible to observe band-edge gain on subpicosecond time scales even for an excitation at 2 eV. Figure 50.30 shows the absorption coefficient measured at 880 nm for various carrier densities. It is clear that  $\alpha$  becomes negative on a subpicosecond time scale for high carrier densities. In fact, gain is observed in a wide spectral region (850–900 nm) on subpicosecond and picosecond time scales for  $N > 3 \times 10^{18} \text{ cm}^{-3}$ .<sup>14</sup> The time delay for gain to occur is  $\sim 280 \pm 80$  fs at 880 nm,  $450 \pm 150$  fs at 860 nm, and  $650 \pm 200$  fs at 850 nm for the highest carrier density ( $N \sim 8\text{--}10 \times 10^{18} \text{ cm}^{-3}$ ) used in these measurements. This time increases to  $\sim 800 \pm 300$  fs at 880 nm and  $> 3000 \pm 800$  fs at 860 nm for lower carrier density ( $N \sim 3.3 \times 10^{18} \text{ cm}^{-3}$ ).

At a probe frequency  $\omega$ , gain should be observed at any given time when the condition

$$\hbar\omega < \mu_{\text{eff}} + E_g \quad (4)$$

with

$$\mu_{\text{eff}} = \frac{m_e + m_h}{\beta_e m_h + \beta_h m_e} (\beta_e \mu_e + \beta_h \mu_h) \quad (5)$$

$$\beta_{e(h)} = \frac{1}{k_B T_{e(h)}} \quad (6)$$

is satisfied. Here  $\mu_{e(h)}$  is the quasi-chemical potential of the  $\Gamma$ -valley electrons (holes) with respect to the conduction (valence) band edge, and  $E_g$  is the normalized band gap. In our model the Coulomb enhancement factor is neglected because of the strong plasma screening at these high carrier densities.<sup>11,29</sup> The calculation of  $\mu_{\text{eff}}$  involves solving a set of kinetic equations for the density and kinetic energy of the  $\Gamma$ -valley electrons and holes.<sup>10,14</sup> Electrons and holes are assumed to equilibrate instantaneously. The initial temperatures of the electrons and holes are  $\sim 3000$  K and  $\sim 600$  K, respectively, based on the kinetic energies of carriers with 2-eV excitation. Scattering to the  $X$  and  $L$  valleys is incorporated into the kinetic model as an energy-dependent sink for the high-energy  $\Gamma$ -valley electrons, again using the effective IDP summarized by Zollner *et al.*<sup>23</sup> Zone-center, LO-phonon emission is also neglected because only a very small amount of energy will be lost by electrons on a subpicosecond time scale when screening is included at high carrier densities.<sup>30</sup> We have compared the calculated delay times for gain to occur using Eqs. (4)–(6) with those deduced from measurements. The hole temperature is treated as a parameter. Good agreement is obtained between model and measurements.<sup>14</sup>

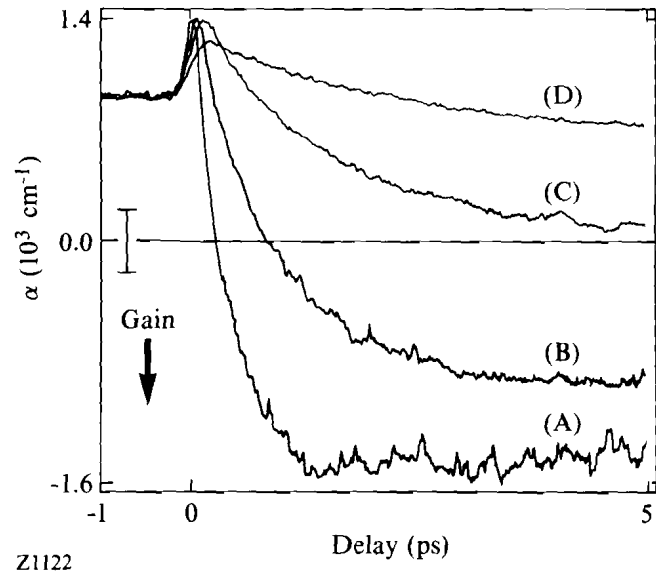


Fig. 50.30

Measured temporal evolution of the absorption coefficient  $\alpha(t)$  at 880 nm for different nominal  $N \sim$ : (A)  $9.0 \times 10^{18} \text{ cm}^{-3}$ , (B)  $3.3 \times 10^{18} \text{ cm}^{-3}$ , (C)  $1.0 \times 10^{18} \text{ cm}^{-3}$ , (D)  $3.3 \times 10^{17} \text{ cm}^{-3}$ . The error bar associated with the uncertainty on the absolute values of  $\alpha$  is indicated.

In addition to revealing the importance of ultrafast equilibration of carriers near the  $\Gamma$  point of the Brillouin zone and the efficient cooling mechanism provided by intervalley scattering, these results also give some insights into hot-hole dynamics. Figure 50.31 displays the hole temperature that gives a best fit to the data. It appears that the hole distribution is heated to  $\sim 800$  K within 300 fs, and then cools down to  $\sim 300$  K within  $<1$  ps. A heated hole distribution indicates that Coulomb-mediated, electron-hole scattering is important on this time scale, in particular when the electron distribution is hotter and for high carrier densities. This result is supported by theoretical calculations including contributions from intervalence and intravalence band scattering processes.<sup>14,31</sup> The rapid “cooling time” of holes that we obtain also agrees well with those measured in *n*-type GaAs using 100-fs time-resolved luminescence.<sup>32</sup>

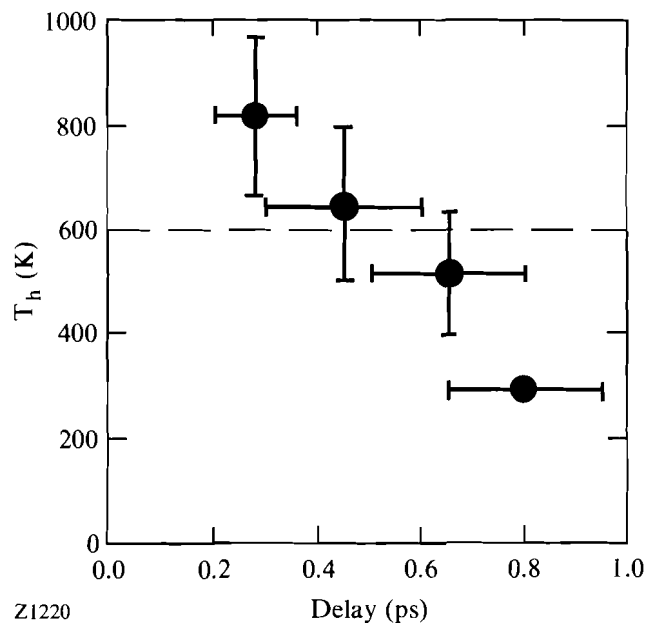


Fig. 50.31

The hole temperature  $T_h$  obtained from the “best fit” between the experiment and the model at different time delays. The dashed line indicates the initial  $T_h$ , based on the kinetic energy of the holes with 2-eV excitation.

### Conclusions

We have performed a series of measurements on time-resolved absorptive and refractive nonlinearities induced by hot carriers injected at 2 eV on GaAs. Measurements near the initial excited states yield the first observation of refractive-index, spectral-hole burning. Studies of spectral-hole burning and initial scattering times reveal the importance of intervalley scattering and carrier-carrier interactions. Measurements near the band edge show that optical nonlinearities on femtosecond and picosecond time scales are governed by various carrier effects, such as band-gap renormalization, plasma screening, band filling, and free-carrier absorption. Subpicosecond gain near the band edge for high injected-carrier densities demonstrates that the rapid cooling of  $\Gamma$ -valley electrons is provided by ultrafast intra- $\Gamma$ -valley equilibration and intervalley scattering. Evidence of a transient heated-hole distribution provides insights for the study of electron-hole and hole-lattice interactions.

## ACKNOWLEDGMENT

We would like to thank J. F. Young and P. J. Kelly at the National Research Council of Canada for performing calculations used in the section on band-edge gain dynamics, and also for many valuable discussions. Contributions from W. L. Nighan, Jr., P. Mertz, C. Peng, M. Shayegan, and G. W. Wicks are also appreciated. This work was supported by the U.S. Army Research Office under Contract DAAL03-91-G-0173, the U.S. Office of Naval Research under Grant N00014-91-J-1488, and the National Science Foundation under Contract ECS-9196000.

## REFERENCES

1. C. V. Shank *et al.*, Phys. Rev. Lett. **42**, 112 (1979).
2. M. J. Rosker, F. W. Wise, and C. L. Tang, Appl. Phys. Lett. **49**, 1726 (1986).
3. J. L. Oudar *et al.*, Phys. Rev. Lett. **55**, 2074 (1985).
4. J. A. Kash, J. C. Tsang, and J. M. Hvam, Phys. Rev. Lett. **54**, 2151 (1985).
5. J. Shah *et al.*, Phys. Rev. Lett. **59**, 2222 (1987).
6. W. Z. Lin *et al.*, IEEE J. Quantum Electron. **24**, 267 (1988), and references therein.
7. P. C. Becker *et al.*, Phys. Rev. Lett. **61**, 1647 (1988).
8. J. A. Kash, Phys. Rev. B **40**, 3455 (1989).
9. X. Q. Zhou *et al.*, Solid State Electron. **32**, 1591 (1989).
10. D. Kim and P. Y. Yu, Phys. Rev. Lett. **64**, 946 (1990).
11. T. Gong, W. L. Nighan, Jr., and P. M. Fauchet, Appl. Phys. Lett. **57**, 2713 (1990).
12. T. Elsaesser *et al.*, Phys. Rev. Lett. **66**, 1757 (1991).
13. T. Gong, P. Mertz, W. L. Nighan, Jr., and P. M. Fauchet, Appl. Phys. Lett. **59**, 721 (1991).
14. T. Gong, P. M. Fauchet, J. F. Young, and P. J. Kelly, Phys. Rev. B **44**, 6542 (1991).
15. E. Yablonovitch *et al.*, Appl. Phys. Lett. **51**, 2222 (1987).
16. C. H. Brito-Cruz, R. L. Fork, and C. V. Shank, in the *XV International Conference on Quantum Electronics Technical Digest Series 1987* (Optical Society of America, Washington, DC, 1987), Vol. 21, p. 82.
17. J.-Y. Bigot *et al.*, Phys. Rev. Lett. **65**, 3429 (1990).
18. D. Hulin (private communication).
19. T. Gong and P. M. Fauchet (unpublished).
20. G. Bohne *et al.*, in the *Technical Digest of the VIIth International Symposium of Ultrafast Processes in Spectroscopy*, Bayreuth, Germany, 7–10 October 1991.
21. P. C. Becker *et al.*, Appl. Phys. Lett. **53**, 2089 (1988).
22. M. A. Alekseev and D. N. Merlin, Phys. Rev. Lett. **65**, 274 (1990); J. A. Kash, J. C. Tsang, and R. G. Ulbrich, Phys. Rev. Lett. **65**, 275 (1990).

23. S. Zollner, S. Gopalan, and M. Cardona, *Solid State Commun.* **76**, 877 (1990).
24. J. C. Tsang and J. A. Kash, *Phys. Rev. B* **34**, 6003 (1986).
25. J. S. Blakemore, *J. Appl. Phys.* **53**, R123 (1982), and references therein.
26. H. C. Casey, Jr. and M. B. Panish, *Heterostructure Lasers, Part A: Fundamental Principles* (Academic Press, San Diego, 1978), p. 175, and references therein.
27. K. Seeger, *Semiconductor Physics* (Springer-Verlag, New York, 1973), p. 379.
28. B. R. Bennett, R. A. Soref, and J. A. Del Alamo, *IEEE J. Quantum Electron.* **26**, 113 (1990).
29. H. Haug and S. W. Koch, *Phys. Rev. A* **39**, 1887 (1989).
30. M. A. Osman and D. K. Ferry, *Phys. Rev. B* **36**, 6018 (1987).
31. J. F. Young, P. Kelly, and N. L. Henry, *Phys. Rev. B* **36**, 4535 (1987).
32. X. Q. Zhou and H. Kurz, in the *Technical Digest of the VIIth International Symposium of Ultrafast Processes in Spectroscopy*, Bayreuth, Germany, 7–10 October 1991; and G. M. Gale *et al.*, *ibid.*